

Key points:

- Simultaneously growing laboratory analogs for hydraulic fractures and dykes interact via their induced stress fields
- Central fractures in uniformly spaced arrays are suppressed when the fracture spacing is sufficiently small relative to the fracture height
- Certain nonuniformly spaced arrays of closely spaced fractures lead to growth of all fractures

Correspondence to:

 A. P. Bunger,
bunger@pitt.edu
Citation:

 Gunaydin, D., Peirce, A. P., & Bunger, A. P. (2021). Laboratory experiments contrasting growth of uniformly and non-uniformly spaced hydraulic fractures. *Journal of Geophysical Research: Solid Earth*, 126, e2020JB020107. <https://doi.org/10.1029/2020JB020107>

 Received 29 APR 2020
 Accepted 15 DEC 2020

Laboratory Experiments Contrasting Growth of Uniformly and Nonuniformly Spaced Hydraulic Fractures

 Delal Gunaydin¹, Anthony P. Peirce², and Andrew P. Bunger^{1,3} 
¹Department of Civil and Environmental Engineering, University of Pittsburgh, Pittsburgh, PA, USA, ²Department of Mathematics, The University of British Columbia, Vancouver, BC, Canada, ³Department of Chemical and Petroleum Engineering, University of Pittsburgh, Pittsburgh, PA, USA

Abstract Hydraulic fractures that grow in close proximity to one another interact and compete for fluid that is injected to the wellbore, leading to dominance of some fractures and suppression of others. This phenomenon is ubiquitously encountered in stimulation of horizontal wells in the petroleum industry and it also bears possible relevance to emplacement of multiple laterally propagating swarms of magma-driven dykes. Motivated by a need to validate mechanical models, this paper focuses on laboratory experiments and their comparison to simulation results for the behavior of multiple, simultaneously growing hydraulic fractures. The experiments entail the propagation of both uniformly and nonuniformly spaced hydraulic fractures by injection of glucose or glycerin-based solutions into transparent (polymethyl methacrylate) blocks. Observed fracture growth is then compared to predictions of a fully coupled, parallel-planar 3D hydraulic fracturing simulator. Results from experiments and simulations confirm the suppression of inner fractures when the spacing between the fractures is uniform. For certain non-uniform spacing, both experiments and simulations show mitigated suppression of the central fractures. Specifically, the middle fracture in a 5-fracture array grows nearly equally to the outer fractures from the beginning of injection. Furthermore, with some delay, the other two fractures that are suppressed with uniformly spaced configurations grow, and eventually achieve a velocity exceeding the other three fractures in the array. Hence, these experiments give the first laboratory evidence of a model-predicted behavior wherein certain nonuniform fracture spacings result in drastic increases in the growth of all fractures within the array.

1. Introduction

Because of major advances in hydraulic fracturing and horizontal drilling technology, vast tracts of gas bearing shale formations have become a significant source of hydrocarbon production in North America and beyond. These formations are called unconventional resources because they cannot be developed and produced by conventional production methods. As a result of their low permeability, higher intensity operations such as drilling a horizontal wellbore in the formation and creating multiple transverse hydraulic fractures crossing this wellbore are essential to make unconventional reservoirs economically viable. Although the type of formation and experience with horizontal wells in a specific formation will dictate the most appropriate type of well completion to be used, a commonality is the use of simultaneous injection into multiple entry points (i.e., clusters of perforation holes made in the casing and cement) with the intent of creating multiple hydraulic fractures in each of multiple, repeated stages (see Figure 1). Typically, each stage comprises three to six perforation clusters, and each stage is repeated 20–40 times on each well. The goal of this completion technique is to generate uniform hydraulic fractures from all perforation clusters within a stage; hence, to create high conductivity pathways to the formation for oil and gas production that uniformly stimulate the reservoir rock. However, industry experience with field data analysis (i.e., production logging during which a flow sensor is moved through the well to measure the contribution of each perforation cluster to the overall production rate) and predictions from simulations make it clear that uniform stimulation can be an elusive goal. For example, Miller et al. (2011) interpreted hundreds of production logs from multiple basins, concluding that approximately two thirds of perforation clusters contribute to well production. Similarly, Molenaar et al. (2012) published one of the first studies using distributed acoustic sensing (DAS) technology with fiber optic cables in a horizontal wellbore, thereby detecting that

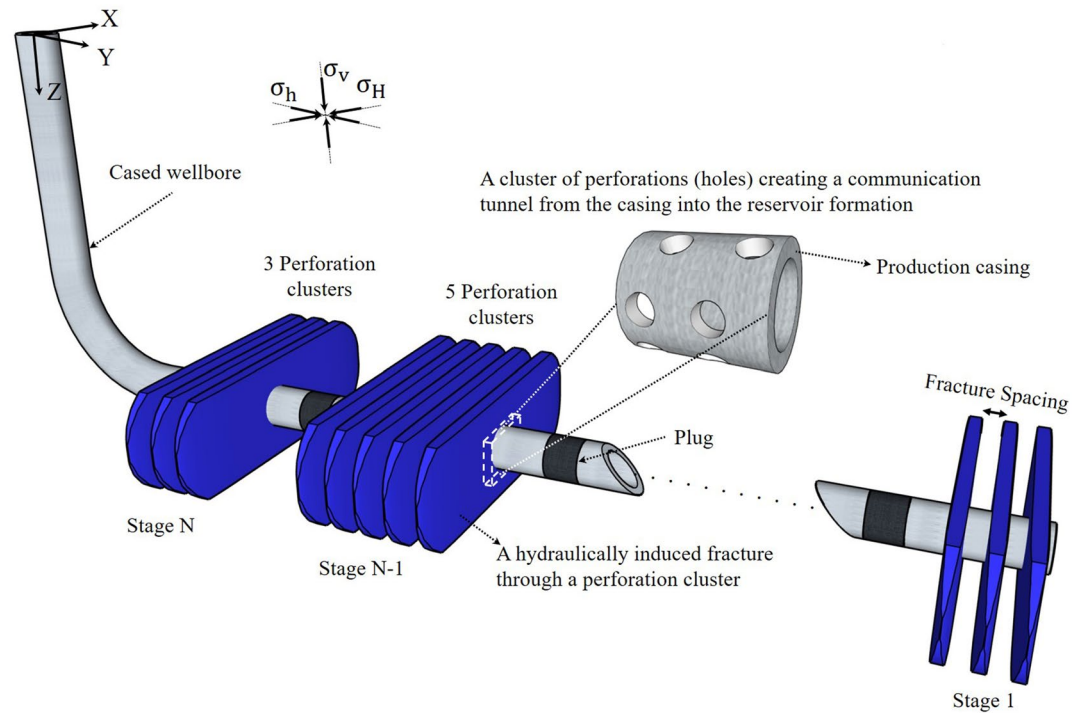


Figure 1. Sketch of a cased horizontal wellbore with multiple hydraulic fracture stages, each containing a different number of perforation clusters (not to scale). The wellbore is drilled in the direction of the minimum horizontal *in situ* stress, σ_h .

only three out of four perforation clusters were effectively stimulated. Similar studies, performed by Mikimins et al. (2014) and Wheaton et al. (2016), indicate that one or two clusters dominate and take most of the fracturing fluid/proppant volume. Finally, Ugueto et al. (2016) conclude that only half or two thirds of the perforation clusters are properly fractured or produced at significant rates after integrating distributed temperature sensing (DTS) and DAS with hydraulic fracture stimulation treatment data for five wells with a total of 120 perforation clusters.

While one contributing factor to nonproducing perforation clusters is the formation heterogeneities including the *in situ* stress variations along the well, another factor is the stress interactions between hydraulic fractures (and indeed other fluid-driven cracks such as dykes) often referred to as “stress shadowing.” When a single fracture is opened, it alters the stress field around it. This perturbation in the surrounding stress regime may emerge as an increased compressive stress exerted on the next fracture in an array of fractures (upcoming nearby fractures) and thereby potentially may affect (i.e., suppress) the growth of these nearby fractures. Early micro-seismic evidence and model-based discussion of this phenomenon is available in the Barnett Shale (Fisher et al., 2004), with more recent evidence from production logs in the Marcellus Shale (Bunger & Cardella, 2015). Furthermore, Wheaton et al. (2016) investigated the effect of spacing on cluster efficiency (i.e., proportion of clusters that are substantially producing). In their study, several stages had perforation clusters which were spaced nonuniformly, approximately two times the distance between the other perforation clusters in the stage. These perforation clusters were observed to be associated with the dominant fractures, presumably because the fractures were less impacted by stresses imposed by neighboring fractures. Fracture models typically predict that the number of fractures that propagate within one stage with multiple perforation clusters is greater than one but generally less than the total number of perforation clusters (Castonguay et al., 2013; Damjanac et al., 2018; Kresse et al., 2013; Lecampion & Desroches, 2015; Meyer & Bazan, 2011; Olson, 2008), with stress interaction (i.e., “stress shadowing”) between fractures a major contributor.

Several optimization studies have been performed to minimize the variations in production from perforation clusters (Cipolla et al., 2011; Salah & Ibrahim, 2018; Slocombe et al., 2013). These studies proved

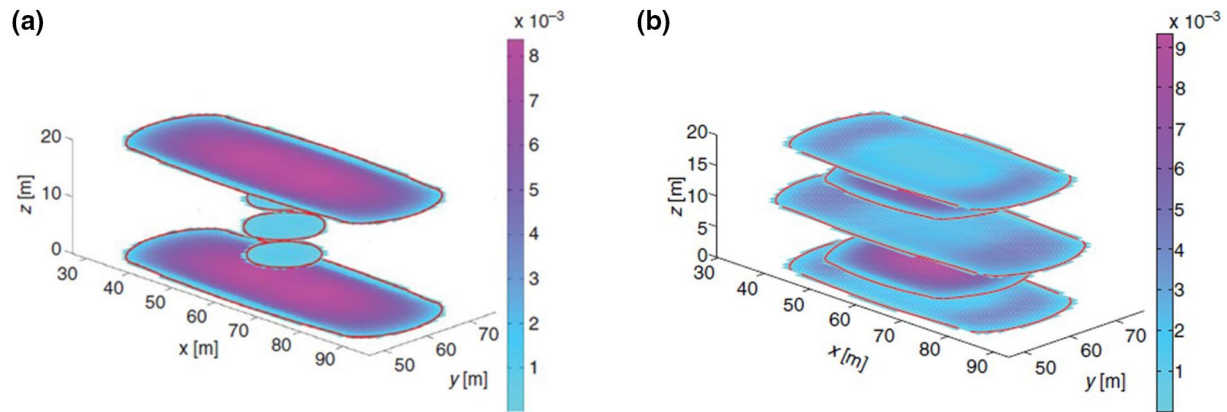


Figure 2. Array of hydraulic fractures with spacing smaller than height, showing results from Implicit Level Set Algorithm (ILSA). (a) Five uniformly spaced hydraulic fractures and (b) five nonuniformly spaced hydraulic fractures. Both results are from Peirce and Bungler (2015), with permission.

the hypothesis that in a lateral well with spatial variation in stress, perforation cluster efficiency can be improved by grouping together stages to be placed in sections of rock with similar stresses for fracturing treatment. That is to say, minimizing naturally occurring stress variability within each stage can improve uniformity of fracture growth. In more recent years, it has become increasingly common to use the so-called “limited entry” methods – which have been used for decades for multi-zonal stimulation of vertical wells (Lagrone & Rasmussen, 1963), but which are now becoming nearly standard practice for promoting growth of simultaneous fractures along horizontal wells. This approach entails using fewer and/or smaller perforation holes per cluster, making the pressure drop through the perforations large enough that it dominates the in situ stress variability and/or fracture interaction stresses, thereby promoting a more uniform distribution of fluid flow to the growing fractures (Lecampion & Desroches, 2015). While often effective, the method comprises a “brute force” approach to the issue that has the effect of substantially increasing the pumping pressure required to create the hydraulic fractures. At best this comprises an increase in cost and decrease in the efficient use of resources that can potentially be avoided by devising lower pressure approaches, built on a fundamental understanding of the mechanics of interacting hydraulic fractures. At worst, reliance on limited entry can render a formation untenable for development if the required treating pressures already approach the limitations of the wellhead and pumping equipment, thereby leaving no capacity in the system for additional limited entry pressure. Hence, the need to understand and model fracture interaction remains vital to ongoing development of hydraulic fracturing technology.

As an example of what might be possible, Peirce and Bungler (2015) investigate multiple fracture propagation at both uniform and nonuniform locations by using a numerical parallel-planar three-dimensional model. They demonstrate that the stress shadow effect on inner fractures can be reduced by appropriately placing them close to the outer fractures instead of placing all the fractures uniformly in an array. Figure 2a shows a snapshot of five numerically modeled hydraulic fractures spaced uniformly at 5 m within a zone that limits the height growth to 20 m (due to higher stress barriers), thereby resulting in a spacing to height ratio of 0.25. The growth is localized in the outer fractures since they have one side that is not subjected to any stress shadow. Inner fractures are clearly suppressed by the growth of outer fractures. However, the result is completely different when the inner fractures are placed in a particular nonuniformly spaced configuration. Figure 2b shows the result when the Fractures 2 and 4 are moved outward to a spacing of 3.6 m from Fractures 1 and 5, respectively, leaving a gap of 6.4 m between them and the center fracture (Number 3). In this case, all five fractures grow substantially due to the equalization of the stress shadowing effect among all fractures.

While it is promising to consider optimizing fracture spacing to minimize negative effects of stress interactions, the required models have relatively scarce validation through comparison to laboratory experiments. That is, despite the fact that interactions between simultaneously growing multiple hydraulic fractures has been widely observed in the field and investigated numerically, the number of laboratory experiments studying same phenomena in the literature is very limited. El Rabaa (1989)’s hydraulic fractures from one

perforation interval experiments, mainly focused on the effect of well deviation and length of perforation intervals on fracture geometry, show that multiple fractures can be created but domination of one fracture over the others is likely to result in nonuniform growth. AlTammar et al. (2018) run experiments to study the effect of changes in pore pressure on multiple hydraulic fracture generation. They created multiple fractures from different holes in the same specimen. These fractures are neither placed in the same wellbore nor do they share a total injected volume of fracturing fluid, since the application of their study is for infill drilling, that is, adding new wells in an existing field within the original well patterns to accelerate recovery.

Here we present results of laboratory experiments conducted to provide a new opportunity to validate models and to observe the effect of stress shadowing on simultaneously growing multiple hydraulic fractures. With the ability to control boundary conditions and material heterogeneity, these experiments are a first step to validate the numerical model simulators that are used to optimize fracture spacing for minimizing the negative impacts of stress shadowing. The experiments are performed in a transparent material. Because the material is transparent, it is possible to measure the evolution of length and height of all fractures based on video images. After describing the experimental method, the results of this experimental study are presented and discussed in light of their ability to provide quantification and visualization of the phenomena resulting from coupled mechanisms associated with development of multiple fluid-driven fractures. Lastly, comparisons are made between experiments and numerical model predictions to emphasize a few of the most eminent growth characteristics of hydraulic fractures in the model versus experiments.

2. Experiments

The analog laboratory experiments are carried out for the purpose of observing the complex interaction among multiple, simultaneously growing fluid-driven fractures in layered geological settings. Obviously, it is impossible to reproduce field scale multiple hydraulic fractures in the laboratory. Additionally, obtaining appropriately scaled investigation of impacts of mechanisms such as hydraulic fracture interaction with natural fractures and/or interplay between fracture growth and transport of granular proppant material in the fluid is beyond the scope of the present work. With that being said, although our experiments do not capture all the physical processes of hydraulic fracturing specific to rock materials, such as heterogeneity and anisotropy, they are similar to field scale hydraulic fractures in that they capture coupling among fluid flow, elastic deformation, and moving boundaries associated with the propagating fracture fronts.

In general, the external energy required to create a hydraulically induced fracture is supplied by fluid injection. Part of this external energy is stored internally in the system by opening the crack. It is also dissipated through three mechanisms: (1) fracturing the rock and making new surfaces (toughness dissipation); (2) friction in the fluid flow (viscous dissipation); (3) fluid loss to the surrounding domain. The fracture propagation depends on the governing energy dissipation process. If most of the energy is dissipated by the creation of new fracture surface, then the growth is dependent upon the rock strength properties such as the fracture toughness and will depend little upon properties associated with fluid dissipation such as viscosity. However, what is often relevant is the opposite case, which is the limiting regime where the dominant energy dissipation is due to fluid flow, as opposed to fracturing the rock. This is the “viscosity-dominated” regime. In this regime, fluid viscosity has a strong impact on fracture growth while rock fracture toughness has little impact (see e.g., the review article Detournay, 2016 for a more complete discussion of these regimes). The experiments in this paper focus on the viscosity-dominated regime. Furthermore, the experiments are performed at the limit where fluid diffusion from the hydraulic fracture to the surrounding rock can be neglected, that is, in the case of infinitesimally small permeability of the rock. Additionally:

- Confining stresses are maintained at a level that is predicted to be sufficient to suppress the so-called “fluid lag” region. Fluid lag refers to the region near the tip of the fracture that is not penetrated by the fracturing fluid and creates the separation between the fluid front and the fracture front. Following prediction of the impact on fracture growth and the ability to suppress it via sufficient confining stress (i.e., stress opposing fracture opening, Garagash & Detournay, 2000), experimental suppression of the fluid lag is promoted through the application of the horizontal stress in these experiments (after Bungler & Detournay, 2008)
- The experiments consider conditions where Reynold’s number is low thus implying laminar fluid flow. Note that although many field treatments are in the transition between laminar and turbulent flow (e.g.,

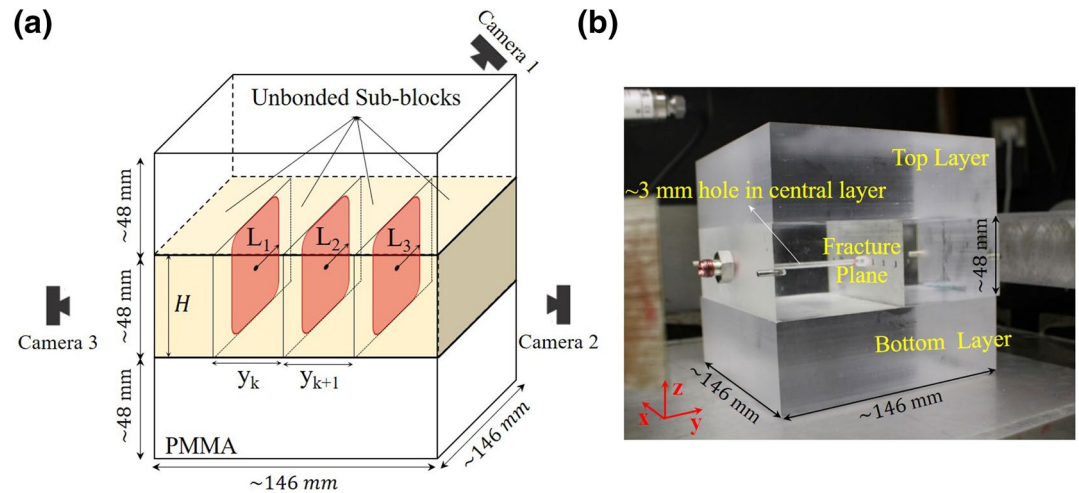


Figure 3. Example specimen composed of three layers, with central layer divided into sub-blocks to observe simultaneous growth of hydraulic fractures. (a) Schematic of a sample specimen illustrating that for N planar fractures with a spacing of y_k , there are $N + 1$ sub-blocks. (b) Picture of a specimen prepared for single fracture growth showing all the unbonded interfaces.

Peirce & Dontsov, 2017; Zia & Lecampion, 2017; Zolfaghari & Bunger, 2019), the laminar flow regime is still often relevant and comprises a useful limiting regime for model validation and field-scale treatment comparison

The experiments consist of creating a series of small-scale hydraulic fractures by injecting Newtonian fluids at controlled rates into transparent rock-analog multi-layered media constructed from polymethyl methacrylate (PMMA), which enables monitoring the growth of hydraulic fractures in real time. The 146 mm cube-shaped specimens are composed of three layers, with central layer subdivided into unbonded sub-blocks. Hydraulic fractures are initiated within the central layer through a 3 mm diameter injection hole. Note that, although the interfaces are unbonded, they are initially pressed closed by the confining stress and must therefore be opened by fluid pressure before they can accept fluid, similar to “zero-toughness” hydraulic fractures that have been widely considered in both experiments (Jeffrey & Bunger, 2009; Xing et al., 2017, 2018), and analysis (Nordgren, 1972; Detournay & Peirce, 2014; Savitski & Detournay, 2002; Simonson et al., 1978).

We consider an array of N planar fractures distributed within the central layer of the PMMA block with a spacing between each fracture organized in an array with components y_k , $k = 1, \dots, N-1$. We let L_k denote the fracture half-length, the maximum distance from the center of the injection hole to the fracture tip at a given time in the k th fracture plane (Figure 3a).

Figure 3b shows a sample specimen with central layer divided into two sub-blocks allowing a single fracture to grow on each x - z plane where the two sub-blocks meet. One reason for using prescribed paths for fractures to grow is to restrict the geometry to planar hydraulic fractures. While hydraulic fractures would, in general, be expected to curve in response to their stress interaction (e.g., Roussel & Sharma, 2011), restricting consideration to planar growth is analogous to the limiting case where the difference between the minimum stress and the other two intermediate stresses is sufficient to suppress curving (see Bunger et al., 2012). By considering this limit, it is possible to isolate behavior that is not associated with curving and thus provide direct comparison to planar computer model results. Of course, introduction of curving would make a useful extension to the present work. In addition, the high strength and fracture toughness of the PMMA can lead to large initiation and propagation pressures that can make it difficult or impossible to design experiments: (1) for which energy dissipation through viscous flow plays an important role in fracture propagation (see e.g., Bunger & Detournay, 2008), and (2) for which the release of compressed fluid in the injection system prior to initiation can be neglected over any portion of the duration of the experiment (see e.g., Lakirouhani et al., 2016; Lhomme et al., 2005). Hence, it is advantageous to initiate the fractures on predetermined interfaces rather than fracturing the blocks themselves.

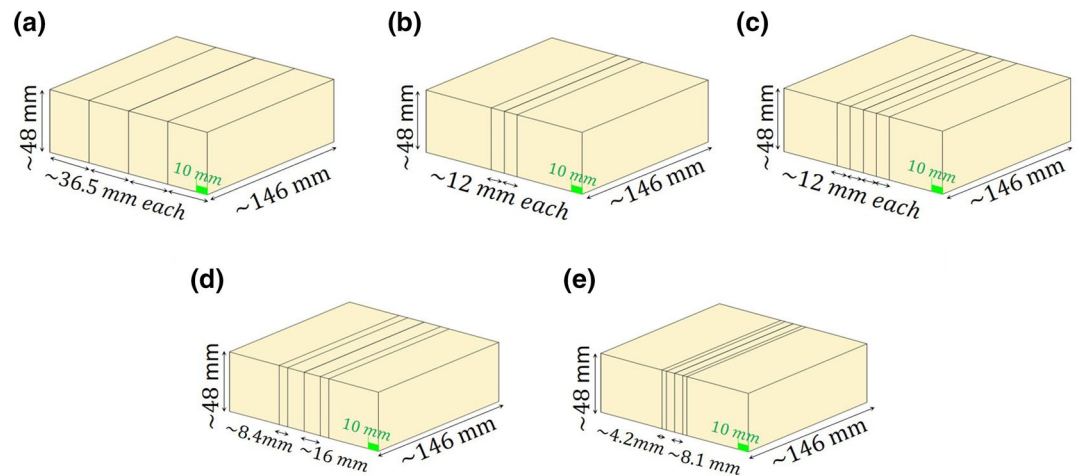


Figure 4. Schematics of central layer of each case are drawn to scale: (a) three uniformly widely spaced fractures, (b) three uniformly narrowly spaced fractures, (c) five uniformly narrowly spaced fractures, (d) five nonuniformly spaced fractures, and (e) five nonuniformly narrowly spaced fractures.

Hydraulic fracture height growth is limited in these experiments in order to be analogous to the common field situation where high stress barrier layers exist. These barrier layers can in general exist above and/or below the reservoir, and they are layers which the in situ stress is larger thereby providing inhibition to upward and/or downward fracture propagation. If barriers are present both above and below the reservoir, and if they have a high enough stress compared to the reservoir to completely suppress vertical growth out of the reservoir, fracture growth is contained in the reservoir, as in the laboratory experiments. Furthermore, with the application of relatively large stress in the vertical direction, the top layer and bottom layer (48 mm each) serve as barriers to fracture growth along the horizontal interface between the layers, again resulting in an analogous geometry to a perfectly contained hydraulic fracture, i.e., one with height growth that is suppressed by barrier layers above and below the reservoir. The height to length ratio of the central layer (~ 3) lets the fractures transition toward the classical blade-shaped – “PKN” after Nordgren (1972) and Perkins and Kern (1961) – hydraulic fracture geometry, as observed previously by Xing et al. (2017).

In each experimental case reported in this paper, the number of sub-blocks and the spacing between their interfaces (of central layer) varies to enable observation of different geometries and behaviors of multiple, simultaneously growing hydraulic fractures. Similar to the numerical simulation study presented by Peirce and Bungler (2015), five different cases have been studied with spacing (between the fractures) to height (of central layer) ratio, y_c/H , varying from 0.09 to 0.76; three uniformly widely spaced fractures, three uniformly narrowly spaced fractures, five uniformly narrowly spaced fractures, five nonuniformly spaced fractures, five nonuniformly narrowly spaced fractures. Schematics of the central layer of each case are drawn to scale in Figure 4.

Fractures are initiated from a manufactured notch at the base of the flat-bottomed injection holes. More details on the sample preparation is given in Appendix A.

As depicted in Figure 5, a loading frame applies horizontal and vertical loads on the specimens with hydraulic actuators in two directions generating horizontal confining stress (σ_h) and vertical confining stress (σ_v). There are two directions of load applied, and the other horizontal direction is free in order to enable observation. It is important, however, to mention that these analog experiments are not most directly relevant to the situation with fractures that are free to curve (rather than restricted to planes) with a negligible intermediate stress. Rather, because the fractures are restricted to growth in planes parallel to its direction of application (as previously discussed), they are better understood as analogs to cases with very large intermediate stress that suppresses the tendency for fracture curving (see Bungler et al., 2012). The applied horizontal load is thus perpendicular to the fracture planes so that the resulting stress is analogous to the minimum horizontal in situ stress. Note that 50.8 mm thick, 304.8 mm long steel plates are connected to the horizontal pistons and a 101.6 mm thick PMMA block is placed on top of the specimens to evenly distribute the load from the actuators to specimens.

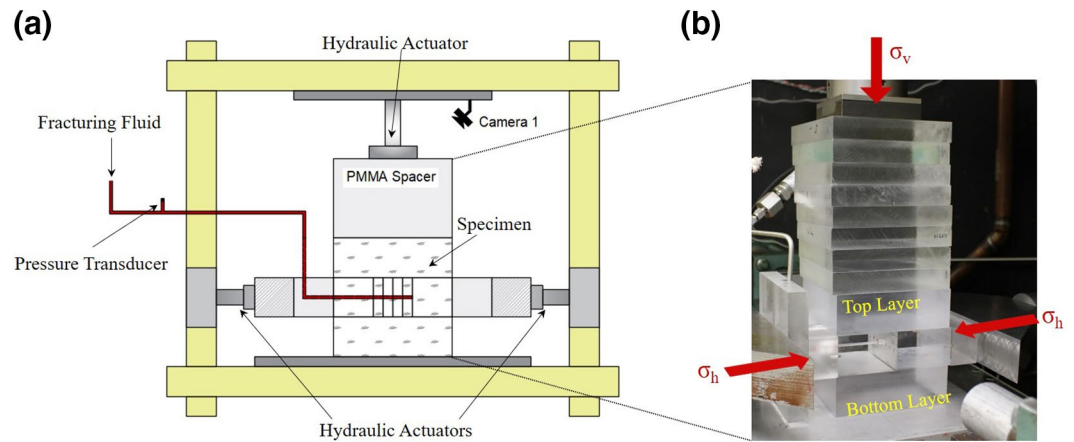


Figure 5. (a) Cross-sectional diagram of the setup for the laboratory experiments and (b) sample subjected to confining stresses in the load frame.

The injected fluid delivered into the central layer by a high-pressure syringe pump (Teledyne ISCO 500D) is composed of glucose with red food dye. At the laboratory temperature of 21°C, the fluid has a viscosity (μ) of 16.5 Pa·s, measured with a Canon-Fenske type capillary viscometer. In the five nonuniformly spaced fractures experiments, glycerin with a viscosity of 0.25 Pa·s is used in alternative cases to the glucose base cases in order to observe the effect of lower viscosity on the multiple fracture-growth patterns. Moreover, in the five nonuniformly narrowly spaced fracture experiments, a new glucose sample is used as injection fluid with a viscosity of 29.3 Pa·s. In all experiments, the injection rate (Q) is kept constant at 2 ml per minute, which results in a total experimental duration on the order of tens of seconds. Table 1 gives a summary of the control parameters and their values used in the experiments. Note that, with the exception of a small pressure drop that could occur along the wellbore due to viscous flow prior to fluid entering the fractures, each fracture inlet is subjected to the same wellbore pressure.

Images of growing fractures are recorded by two or three video cameras, depending on what is required to give images of advancing tips for all fractures. The three-camera configuration consists of two digital single-lens reflect (DSLR) cameras (at speeds of 24 and 30 frames per second) and an action camera (with a 30 frames per second rate) recording the experiments. Ambient room lighting is eliminated by performing experiments in a dark room. A uniform, green-filtered light is set on the side of the specimen as the only lighting source. Camera 1 is placed next to the vertical piston facing the top plane of the specimen with an approximately 45° angle, thereby recording growth in the length of each growing fracture. Meanwhile, Cameras 2 and 3 are placed on the sides of the block to record height growth of each fracture. Recorded videos of each experiment are synced by using reference audio and time delay analysis. Synced videos are then transformed into red-green-blue (RGB) images. By using Image J, a public domain Java image processing program, the RGB images are analyzed to plot the time-evolution of each fracture's growth. In addition to image data, confining stresses and fluid pressure are also logged during all the experiments.

In all cases, one representative experiment is presented. However, each case was carried out 3–5 times in order to ensure repeatability. For each repeat, the blocks were removed, cleaned, and replaced in a different order to ensure that the observed behaviors are not caused by detailed differences between subblocks (or possible creep-related permanent deformation of the PMMA) that are inevitable in reality in spite of utmost care being taken to cut, machine to size, and drill holes identically from one subblock to another.

3. Results

For each case, we present frames of videos recorded by Camera 1 and Camera 2 at different times. For the sake of brevity, these reported times can be referred to as early time, middle time, and late time of the experiments. For all the reported experiments, early time represents the period when the fractures are already in-

Table 1
Summary of Control Parameters

Experiment cases	Material	Fluid	N	y_k (mm) [$k = 1, \dots, N-1$]	H (mm)	μ (Pa·s)	Q (ml/min)	σ_v (MPa)	σ_h (MPa)
Three Uniformly Widely	PMMA	Glucose	3	$y_1 = y_2 = 36.5$	48	16.5	2	12	1.5
Three Uniformly Narrowly	PMMA	Glucose	3	$y_1 = y_2 = 12$	48	16.5	2	12	1.6
Five Uniformly Narrowly	PMMA	Glucose	5	$y_1 = y_2 = 12$ $y_3 = y_4 = 12$	48	16.5	2	12	1.6
Five Nonuniformly	PMMA	Glucose	5	$y_1 = y_4 = 8.4$ $y_2 = y_3 = 16$	48	16.5	2	16	1.6
Five Nonuniformly	PMMA	Glycerin	5	$y_1 = y_4 = 8.4$ $y_2 = y_3 = 16$	48	0.25	2	15	1.6
Five Nonuniformly Narrowly	PMMA	Glucose	5	$y_1 = y_4 = 4.4$ $y_2 = y_3 = 7.9$	48	29.3	2	19	1.7

Note. In addition to image data, confining stresses and fluid pressure are also logged during all the experiments. PMMA, polymethyl methacrylate.

initiated, small, and growing almost radially. During the middle time, at least one fracture encounters the vertical stress barriers, that is, upper and/or lower boundaries. Finally, late time snapshots show the fractures towards the end of the experiments as the longest fracture approaches the edge of the block. It is important to note that these snapshots in the following figures are given in three rows. While each row represents the time, the first column shows the frames of Camera 1 and, subsequent columns belong to Camera 2 and schematic views of the fractures. In addition to the qualitative results, fluid pressures and quantitative data of height and length growth of each fracture are given as average half lengths and average half heights. In the experiments, a fracture is created that propagates with two wings being 180° apart. Considering there are two wings per fracture, average half-lengths and average half heights provided in this paper are estimated by averaging lengths and heights of two corresponding wings of a fracture. Additionally, maximum and minimum values of the final average half-length of each fracture obtained from the repeated experiments are provided on the average half-length plots to show the range of results among the repeated experiments.

3.1. Three Uniformly Widely Spaced Fractures

First, we consider the case in which the central layer of the specimen is divided into four sub-blocks to accommodate three hydraulic fractures (Figure 4a). Each sub-block is ~ 36.5 mm wide resulting in a spacing to height ratio of 0.76. Spacing between the fractures are 36.5 mm (henceforth, denoted 36.5–36.5 mm spaces). Images of the growing fractures and corresponding plots of fluid pressure, length and height are shown in Figure 6. The data are presented from the first moment at which a fracture was visible until at least one wing of a fracture reaches the end of the PMMA block. Figure 6 shows the perspective snapshots of both cameras at times $t = 45, 55,$ and 70 s. The first fracture, described as Frac-1 in Figure 6a, initiates before the others and hits the vertical boundaries first. As can be seen in Figure 6c, by the time Frac-1 reached the end of the PMMA cube in the x -direction, Frac-2 and Frac-3 are still growing.

In addition to the visual results, the time evolution data of height and length growth of each fracture and the fluid pressures are given in Figure 6. While Figure 6d shows the fracture half-lengths and fluid pressures, Figure 6e represents the height growth and the length to height ratio of each fracture. Both figures show the dominance of Frac-1 over the other two fractures. The results do not show a clear suppression of middle fracture, Frac-2, by outer fractures. Rather, these indicate dominance of the fracture that is nearest the injection point, possibly indicating that pressure loss as the fluid flow through the central hole from one inlet to another is the predominant determinant of which fracture grows most rapidly. Estimates based on classical equations for laminar flow (see Appendix B) flow in circular pipes suggests pressure loss as the fluid reaches the third fracture compared to the first fracture to be around 0.02 MPa. In the following experiments, the pressure drop as the fluid reaches the last fracture in the array is estimated between 0.006 MPa and 0.01 MPa. Similar behavior is shown (albeit in cases with four fractures) in simulations by Lecampion and Desroches (2015). For experiments with more closely spaced fractures, it seems this pressure drop is negligible compared to the stresses driving fracture interaction. However, in this case with more widely separated fractures, this small perturbation appears to be enough to favor growth of the fracture that is nearest the pump.

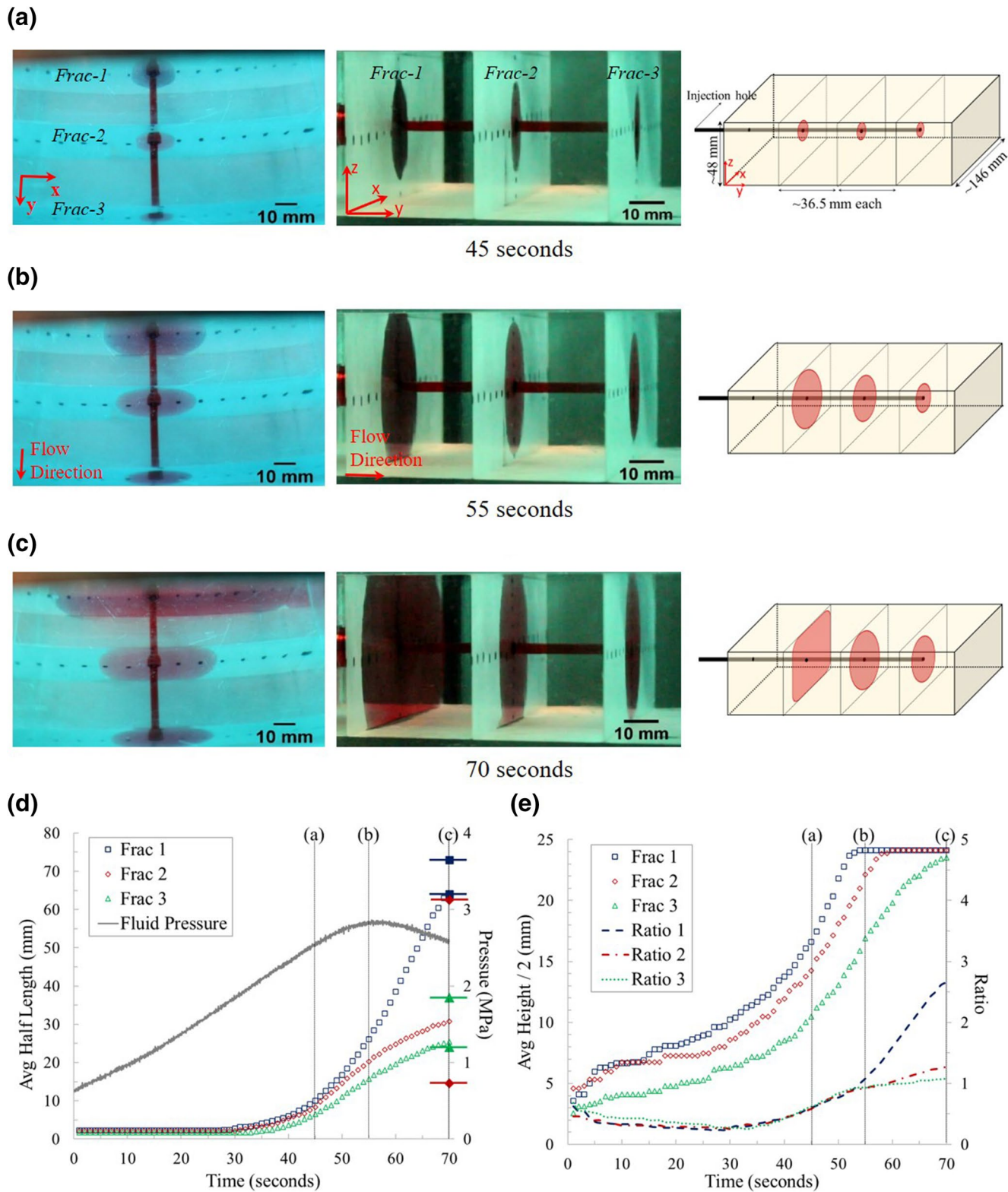


Figure 6. Images of Cameras 1 and 2 of three uniformly widely spaced fractures at different times are shown in (a), (b), and (c). While Camera 1 recorded the growing fractures from the top of the polymethyl methacrylate (PMMA) block, Camera 2 recorded them from the side, (d) average fracture half-length versus time plot is obtained from the video recorded by Camera 1. Maximum and minimum half-lengths of each fracture, given on the plot as marked points, is obtained from repeated experiments, (e) video recorded by Camera 2 is analyzed to plot average fracture half height versus time data.

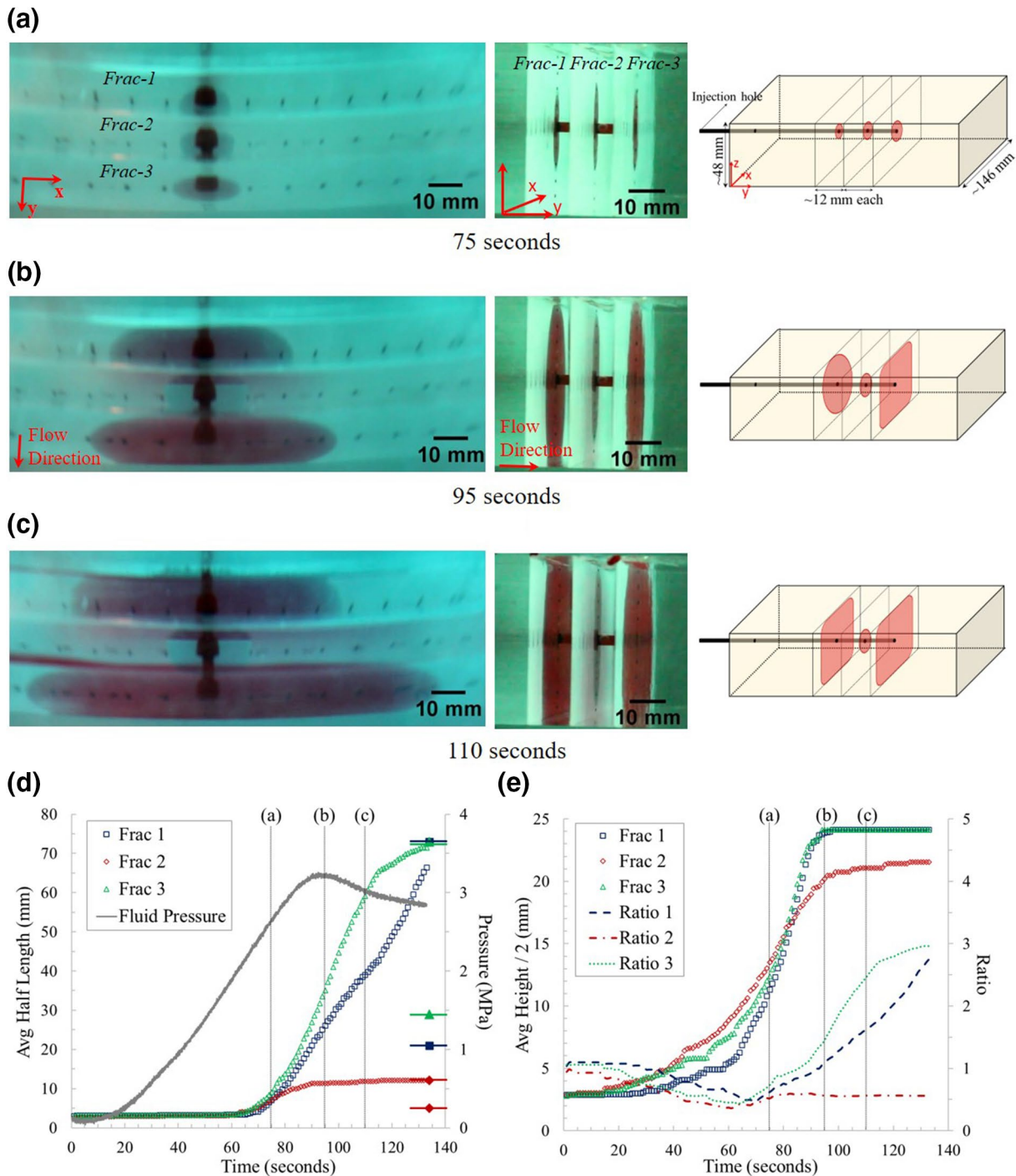


Figure 7. Images of three uniformly narrowly spaced fractures at different times are presented in (a), (b), and (c). Images on the left belong to Camera 1 recording the growing fractures from the top of the polymethyl methacrylate (PMMA) block and images on the right are from Camera 2 used to record the experiment from the side. (d) Average fracture half-length and fluid pressure versus time. Maximum and minimum half-lengths of each fracture, shown as marked points, are obtained from repeated experiments, (e) average fracture half height versus time.

3.2. Three Uniformly Narrowly Spaced Fractures

Now, we consider the case where the spacing between the sub-blocks are reduced from 36.5 mm to 12 mm resulting in a spacing to height ratio of 0.25 ($y_1 = y_2 = 12$ mm; denoted as 12–12 mm spaces, Figure 4b). All three fractures start in a radial geometry with length to height ratio of one (see Figure 7a and Figure 7e).

Around 15 s, the ratios start to reduce from unity indicating that fractures grow in z -direction (vertically) faster than they do in the x -direction. Outer fractures encounter the vertical stress barriers around 90 s and start to transition to blade like geometries resulting in preferred growth in the x -direction (horizontally) and hence to length to height ratios greater than one (Figure 7 b). The middle fracture does not develop at the same rate, presumably because of the mutual stress interaction among the three fractures leading to a higher compressive stress region in the middle of the array. As predicted by hydraulic fracture models, the localization of growth on the outer fractures become dominant towards the end of the experiment as shown in Figure 7c. Evidence of middle fracture suppression by outer fractures due to stress shadowing is apparent at the end of the experiment with a final average half-length of middle fracture to outer fractures ratio of around 1:7 (Figure 7d).

3.3. Five Uniformly Narrowly Spaced Fractures

In the previous experiment of three uniformly narrowly spaced fractures, the spacing to height ratio is 0.25. Keeping the spacing same for five uniformly spaced fractures ($y_1 = y_2 = y_3 = y_4 = 12$ mm; denoted as 12–12–12–12 mm spaces) resulted in clear dominance by the outer fractures of the middle fractures' growth. Initially, fractures show radial growth (Figure 8a) with a length to height ratio of about one (Figure 8e). However, around 10 s into the experiment, they grow faster in the z -direction (vertically). The outer fractures of the five-fracture array, Frac-1 and Frac-5 hit the vertical boundaries around 85 s (Figure 8b) and preferentially grow in the x -direction (horizontally) and eventually transition to blade-like geometries. Furthermore, the fluid pressure peaks around 85 s (Figure 8d). As expected, the fracture growth is localized in the outer fractures, evidencing suppression of the growth of inner fractures. Because Frac-1 and Frac-5 do not have nearby fractures to one side, they have less induced compressive stress from neighbors and hence less constraint on their growth. Meanwhile, interior fractures, Frac-2, Frac-3, and Frac-4, compete to grow under the stress shadowing caused by the outer fractures. The effect of the stress interaction among five fractures appears to increase throughout the experiment (Figure 8c).

Figures 8d and 8e show time evolution plots of half-length and half-height data for each fracture. On both plots, the curves of Frac-1 and Frac-5 are nearly indistinguishable. Although the length growth of Frac-2 and Frac-4 is nearly identical, Frac-4 is slightly shorter than Frac-2 at the end of the experiment. In addition, it is clear from Figure 8e that the outer fractures hit the vertical stress barriers and continue to grow in the x -dimension, resulting a length to height ratio larger than one, whereas the inner fractures do not grow sufficiently to be affected by the vertical boundaries. At the end of the experiment, the middle fracture, Frac-3, is slightly bigger than its neighbors, Frac-2 and Frac-4. However, it is still apparently suppressed by the increase of the compressive stress field in the inner fracture region caused by outer fractures, but perhaps this suppression is slightly less pronounced because it is not a nearest neighbor to the largest, and hence largest stress-producing fractures, Frac-1 and Frac-5. Furthermore, we note that the width (aperture) of Frac-4 may be less, based on the observation that it blocks less light passing through, however, because of the reflections, high camera angles, and obstructed views from other fractures, it is not possible here to carry out quantitative photometric measurements (e.g., Bunger, 2006).

3.4. Five Nonuniformly Spaced Fractures

For this experiment, a modification is made to the uniform case by changing the spacing such that Frac-2 and Frac-4 are closer to the outer fractures, resulting in $y_1 = 8.4$ mm, $y_2 = 16$ mm, $y_3 = 16$ mm and $y_4 = 8.4$ mm (as a shorthand, 8.4–16–16–8.4 mm spaces). This particular spacing is obtained by re-scaling the spacing predicted to generate more uniform growth by Peirce and Bunger (2015).

Figure 9 shows perspective snapshots of these nonuniformly spaced fractures at times $t = 20, 35,$ and 60 s. The vertical lines, 10-mm apart, and the horizontal lines, 5-mm apart, are drawn on the fracture planes for time evolution plots. Figure 9a corresponds to a time when all the fractures are relatively similar in size. Around 35 s into the experiment, images in Figure 9b indicate that extension of Frac-3 and Frac-5 are larger compared to the inner fractures, 2 and 4.

Comparing the Frac-3 of the five uniformly narrowly spaced fractures experiment (Figures 8d and 8e), to the Frac-3 of the current case (Figures 9d and 9e), one can see the effect of placing Frac-2 and Frac-4 nearer

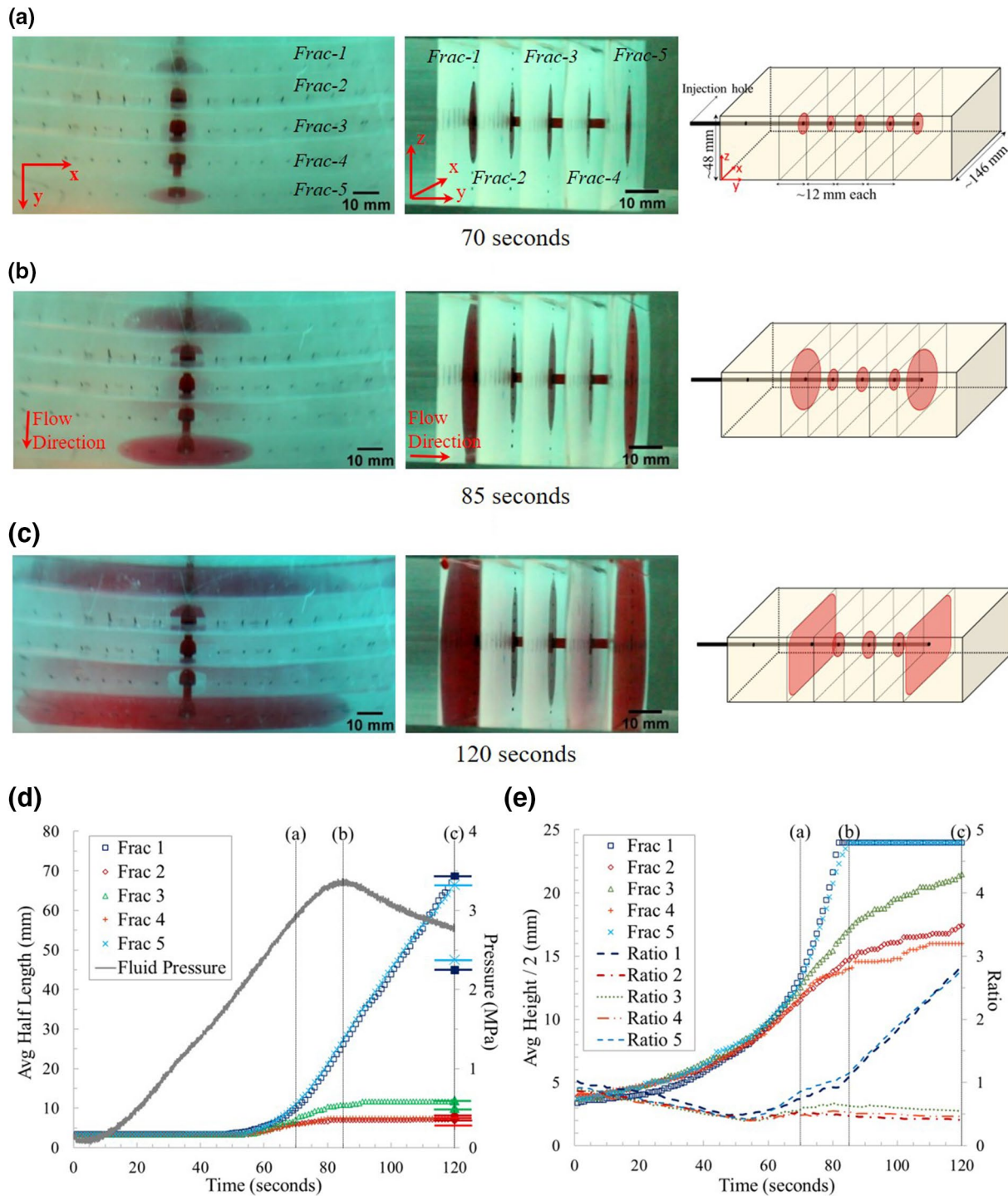


Figure 8. (a), (b), and (c) Images from Cameras 1 and 2 of five uniformly narrowly spaced fractures at different times. While Camera 1 recorded the growing fractures from the top of the polymethyl methacrylate (PMMA) block, Camera 2 recorded them from the side, (d) average fracture half-length versus time plot shows that the outer fractures suppressed the inner fractures. Marked points represent the maximum and minimum avg. half-length of each fracture from repeated experiments. (e) Average fracture half height versus time.

to the outer fractures. These two fractures are dubbed “interference fractures” by Peirce and Bungler (2015) because their close proximity to Frac-1 and Frac-5 serves to create a more even distribution of stress interference among the fractures, thus slowing the growth of Frac-1 and Frac-5 and promoting the growth of

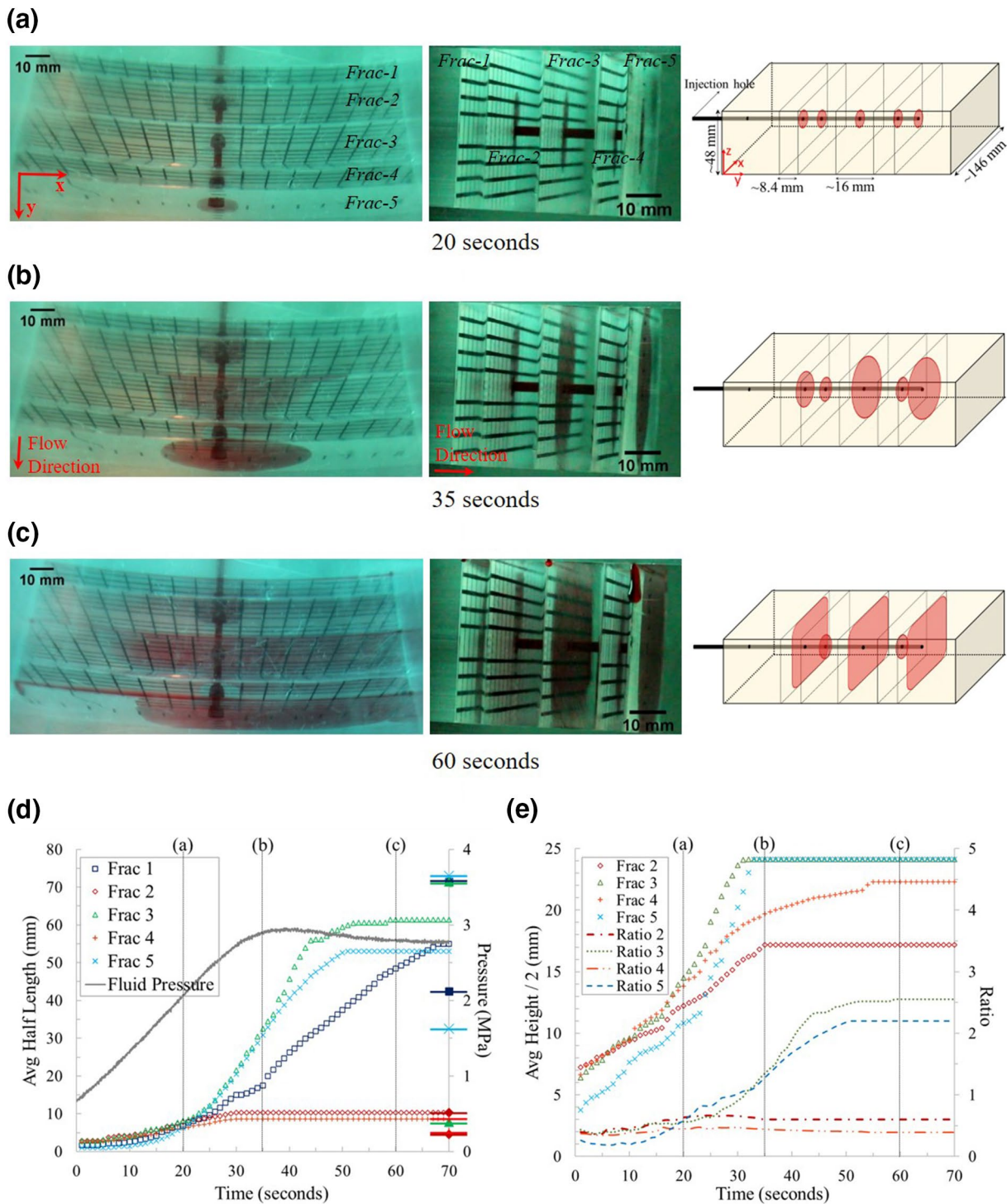


Figure 9. Snapshots of five nonuniformly spaced fractures at different times are given in (a), (b), and (c). Images on the left belong to Camera 1 recording the growing fractures from the top of the polymethyl methacrylate (PMMA) block and images on the right are from Camera 2 used to record the experiment from the side. (d) Average fracture half-length and fluid pressure versus time plot with minimum and maximum half-lengths of each fracture obtained from repeated experiments, (e) Average fracture half height versus time.

Frac-3. Indeed, in the experiments, by bringing the interference fractures closer to the outer fractures, Frac-3 grew larger both in height and length compared to Frac-3 in the uniformly spaced case. Also, both Frac-2 and Frac-4 for the nonuniformly spaced case are larger by the end of the experiment than these fractures were in the uniformly spaced case.

Another observation on the length images of this experiment is that the fracture growth is skewed to right side of the injection hole. The possible explanation for this asymmetrical growth is that the steel plate attached to the vertical piston was not fully centered on the PMMA block during this experiment. While loading the experiment sample with the vertical piston, visibility of fracture growths for Camera 1 was prioritized. Although the same phenomenon is observed in other cases, the preferential growth on one side is more prominent in this experiment, potentially pointing to a higher sensitivity of the fracture growth to perturbations in loading symmetry compared to other cases (i.e., due to positive feedback between closely spaced fractures that could enhance instabilities).

3.4.1. Five Nonuniformly Spaced Fractures with Lower Viscosity Fluid

In this experiment, viscosity of the fracturing fluid is reduced from 16.5 Pa-s to 0.25 Pa-s by changing it from glucose to glycerin in order to observe the effect of viscosity on fracture growths in the five nonuniformly spaced fractures case (8.4–16–16–8.4 mm spaces). Lower viscosity can be expected to generate smaller fluid pressure and hence smaller fracture width and larger fracture length compared to higher viscosity cases with the same volume of fluid injected into the same material in the same period of time. Smaller fluid pressure and smaller fracture width both lead to smaller interaction stress (e.g., [Bunger et al., 2013](#); [Cheng & Bunger, 2019](#)). So, on the one hand, smaller viscosity might lead to smaller level of suppression of fractures due to stress interaction. However, on the other hand, larger viscosity can lead to geometric stability in hydraulic fracture growth ([Bunger, 2005](#); [Gao & Rice, 1987](#)). Hence, a question becomes whether the effect of stress shadowing on inner fractures will be diminished by reducing the viscosity of the injection fluid while keeping the other parameters of the experiment setup such as the current spacing to height ratio constant.

Figure 10 contains a composite of nine video images of fracture growths. The first column of images in Figures 10a–10c is taken by Camera 1 showing the top view of the PMMA block; images on the second column belong to Camera 2 and third column displays sketches representing growth of each fracture based on the videos obtained from three cameras. An additional camera, Camera 3, is used in this experiment to observe the height growth of Frac-1 since Camera 2 cannot capture it due to its close proximity to the first fracture. Note the geometry of the fractures being trapezoidal in footprint in Figures 10b and 10c is unexpected but consistently observed in repeated experiments.

Another difference observed in this experiment is the time and the growth rate of fractures. A majority of the length growth starts after fractures reach the vertical boundaries (i.e., the top and bottom blocks providing the limits on height growth, see Figure 3), at around 125 s (Figure 10d). Moreover, it is interesting to note that fractures initiate in succession such that Frac-1 initiates first, Frac-2 initiates at 7 s into the experiment, Frac-3 starts to grow 24 s after the start of the experiment and finally Frac-5 initiates at 48 s, as shown in Figure 10e. Note that the height versus time data of Frac-4 could not be obtained due to the closeness of Frac-4 to Frac-5 and the practical limitations on the angles available for viewing.

Reducing the viscosity of injection fluid by changing it from glucose to glycerin led to larger Frac-2 and Frac-4 by the end of the experiment than these fractures were in the previous case (five nonuniformly spaced fractures). Furthermore, Figure 10e shows that all the fractures in this case grow entirely in the vertical direction. Except Frac-1, the overall growth, i.e. total height and length of each fracture by the end of the experiment, of the rest of the fractures are similar. So, on the one hand, reducing the viscosity causes a geometric instability in the fractures and consequently makes the lateral growth less than expected. On the other hand, it still helps to reduce the interaction between the fractures resulting in more uniform growth between Frac-2, Frac-3, Frac-4, and Frac-5. Additionally, the pressure in this experiment is unexpectedly higher than in the comparable experiment with higher viscosity. The reason for this higher pressure is unclear, although it is important to point out that multiple fracture cases have complicated coupling among fractures so that hypotheses based on single fracture behavior may not necessarily hold.

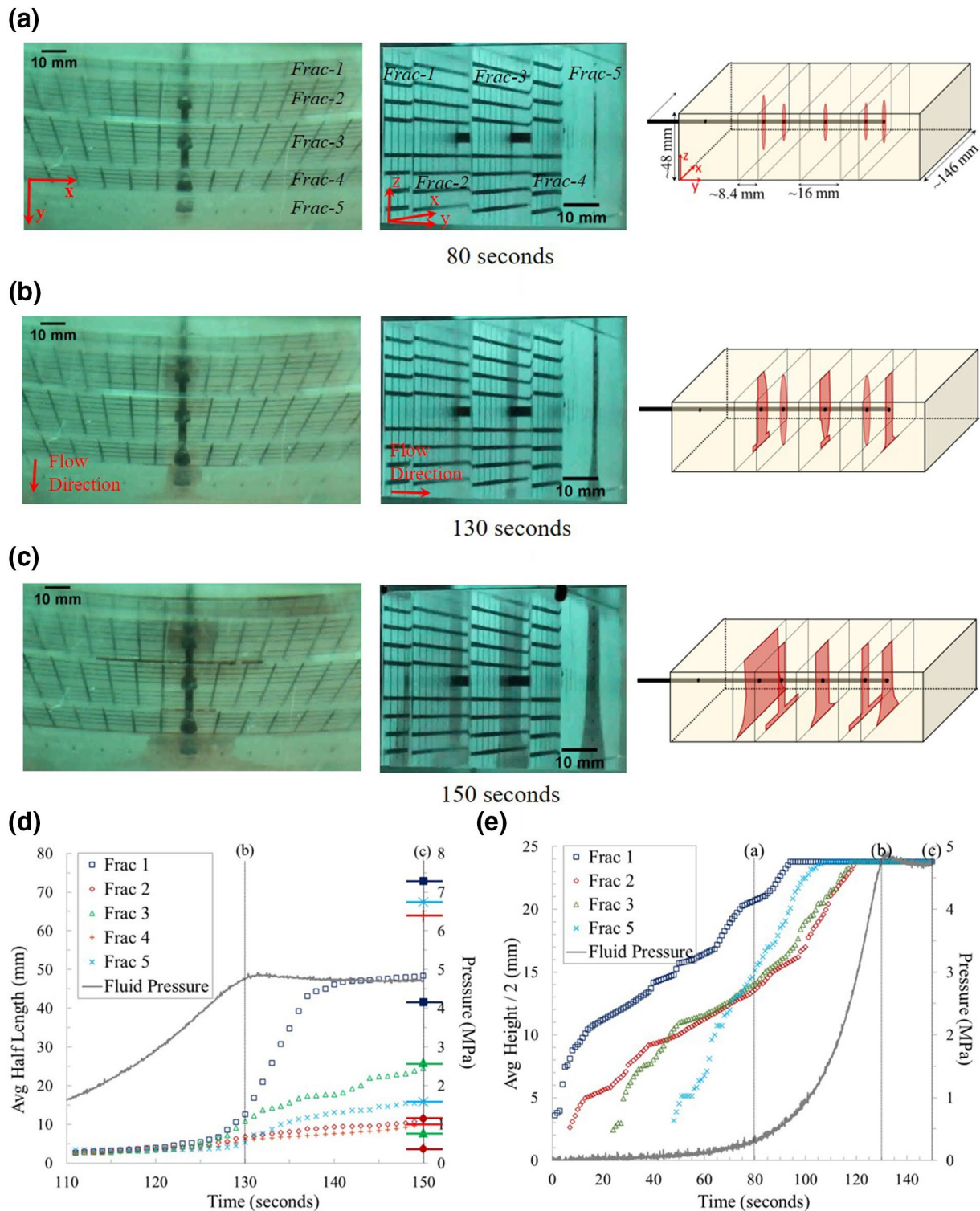


Figure 10. Images of the five nonuniformly spaced fracture experiment with glycerin injection, at times: (a) 80 s, (b) 130 s, (c) 150 s. Images are obtained from three cameras. While Camera 1 recorded the growing fractures from the top of the polymethyl methacrylate (PMMA) block, Camera 2 recorded them from the right-side and Camera 3 from the left-side, (d) Average fracture half-length versus time plot is obtained from the video recorded by Camera 1. Maximum and minimum half-lengths of each fracture, given on the plot as marked points, are obtained from repeated experiments, (e) videos recorded by Cameras 2 and 3 are analyzed to plot average fracture half height versus time data.

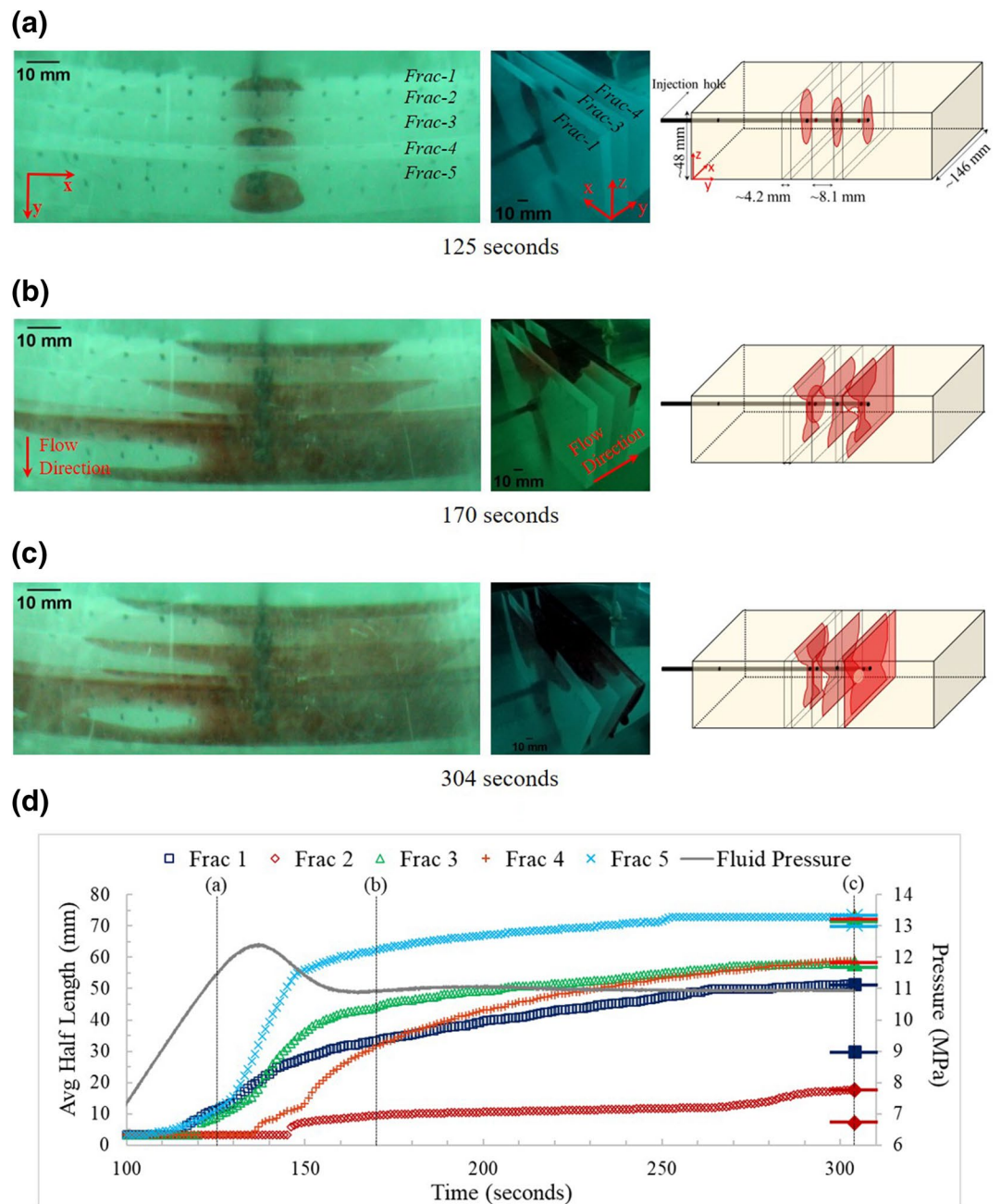


Figure 11. Images of five nonuniformly distributed narrow fractures at different times are given in (a), (b), and (c). Images are obtained from three cameras. While Camera 1 recorded the growing fractures from the top of the polymethyl methacrylate (PMMA) block, Camera 2 recorded them from the right-side and Camera 3 from the left-side. (d) Average fracture half-length versus time plot is obtained from the video recorded by Camera 1. Maximum and minimum half-lengths of each fracture, shown as marked points on the plot, are obtained from repeated experiments.

3.5. Five Nonuniformly Narrowly Spaced Fractures

This experiment has also five nonuniformly spaced fractures, however, the spacing between Fractures 2, 3, and 4 are reduced approximately by half such that $y_1 = y_4 = 4.2$ mm, and $y_2 = y_3 = 8.1$ mm while keeping the height of the fractures same at 48 mm (4.2–8.1–8.1–4.2 mm spaces, Figure 4e). Glucose with a viscosity of 29.3 Pa s is pumped to generate the fractures. Figure 11 shows fracture growths in six video images, and three sketches. Videos obtained from four cameras are used to prepare the sketches.

Figure 11a, showing early time images at 125 s, demonstrates that outer fractures and middle fracture started to grow with similar lengths. This is unlike the uniform-spacing cases, where outer fractures suppress the growth of inner fractures, commencing the suppression as soon as the fracture length and/or height attains a value similar to the fracture spacing, that is, even at early time in the experimental progression. The different behavior is further apparent by examining the evolution of the fracture lengths shown in Figure 8d for the uniform spacing in contrast to Figure 11d for the nonuniform spacing.

While these three fractures, Frac-1, Frac-3, and Frac-5 show robust growth from the beginning of the experiment, the half-length of Frac-4 accelerates and then exceeds the half-length of Frac-1 around 175 s into the experiment, (Figure 11d). By the end of the experiment, the overall behavior of all fractures except Frac-2 shows similar levels of growth, indicating a tendency to uniform growth of the fracture array that is apparently not present in other cases. Although the half-length of Frac-2 is smaller compared to the rest of the fractures at the end of the experiment, it is still longer than half-lengths of Frac-2s of previous experiments.

One striking comparison is the sum of all of the fracture half lengths. Table 2 shows the final average half-length of every one of fractures measured at the end of each experiment and their sum. Because fracture height is fixed, a change in this sum of half-lengths is directly proportional to the fracture surface area. In turn fracture surface area is widely believed to be directly related to the production that can be expected from hydraulic fracture stimulation. Here, the final total of the fracture half lengths of the current case compared with the five uniformly narrowly spaced fractures case is increased by 60%. It is, however, important to note that the total injected volume of each experiment varies because the duration of each experiment is different. The duration of these experiments is determined not by a fixed injection time but rather by the time it takes for the longest fracture to reach the lateral boundary of the specimen. In five uniformly narrowly spaced fractures experiment, it takes 120 s for Frac-1 (the longest in this case) to hit the lateral boundary (Figure 8c), whereas it takes 250 s in the experiment of five nonuniformly narrowly spaced fractures (Figure 11d). Practically speaking, this indicates that more uniform stimulation of every fracture allows a longer injection time and more total (summed) fracture length when the constraint on growth is the length of the longest fracture. This scenario is similar to a case where injection time is limited in a field application by the time it takes to receive indication that at least one growing fracture is providing a pressure response on an offset well, as is often the case when stimulating multiple wells that are drilled from a single well pad.

Another observation from this experiment is that the range of fluid pressure is higher compared to the other experiments (see Figure 11d). One reason might be the slightly higher viscosity fluid that is injected during this experiment (29.3 Pa s in contrast with 16.5 Pa s). In addition, the horizontal stress applied on the sample during this experiment is also moderately higher than the stresses of previous cases. With that being said, the impact of the viscosity difference and accompanying slight increase in pressure appears to be slight. Specifically, simulations with 16.5 Pa s (omitted for brevity) indicate similar behavior of Fractures 2 and 4 to the 29.3 Pa s case, with the only notable difference being slightly greater relative growth of fracture 3 in the lower viscosity simulation. Furthermore, note that there is a slight increase in pressure just after point b in Figure 11d. Such a pressure increase is also observed to coincide with the mobilization of fractures 2 and 4 in the simulations of Peirce and Bungler (2015).

4. Comparison to Numerical Model

This section presents comparison between the results of three experiments and predictions of a numerical model. A detailed comparison of every experiment presented in this paper with multiple simulators would comprise a major effort that is beyond the current scope of this paper which we want to keep focused on the experiments. However, it is illustrative to add a few of the most prominent behaviors and how they behave in simulations versus experiments. For this purpose, we use ILSA II, a parallel-planar three-dimensional hydraulic fracturing simulator that includes full coupling between fluid flow, fracture growth, and elastic deformation of the rock by means of Implicit Level Set algorithm (ILSA) developed by Peirce and Detournay (2008). Details of the adaptation of ILSA to enable simulation of multiple parallel hydraulic fractures (ILSA II) are described by Peirce and Bungler (2015). So, without repeating these details here, we use ILSA II as a fully coupled simulator for comparison with experiments.

For this comparison, we focus on three cases:

Table 2
Final Average Half-Length of Every One of Fracture Measured at the End of Each Experiment

Experiment cases	Frac-1 (mm)	Frac-2 (mm)	Frac-3 (mm)	Frac-4 (mm)	Frac-5 (mm)	Sum (mm)
Three Uniformly Widely	64	31	25	–	–	120
Three Uniformly Narrowly	66	12	71	–	–	150
Five Uniformly Narrowly	69	7	12	7	66	161
Five Nonuniformly	55	10	61	9	53	188
Five Nonuniformly (glycerin)	48	11	24	10	16	110
Five Nonuniformly narrowly	51	18	58	59	73	259

- 1) Five uniformly narrowly spaced fractures, where experiments show suppression of the three inner fractures with central fracture three slightly longer than Fractures 2 and 4
- 2) Five nonuniformly spaced fractures, where concurrent growth of Fracture 3 is observed along with Fractures 1 and 5
- 3) Five nonuniformly narrowly spaced fractures, where Fractures 3, 1, and 5 dominate early on and Fractures 2 and 4 begin to grow later in the experiment

The dimensions and boundary conditions of the simulation runs are the same as experiments. Young's Modulus is set to 3.17 GPa. Poisson's ratio is 0.35. The fluid viscosity is 16.5 Pa·s for the first two cases and 29.3 Pa·s for the third case, again, matching experimental conditions. The nominal injection rate is 2 ml/min. Fracture height and spacing between fractures are also chosen in each case to match the experiments.

While the model is set to match the experiments to the best of its ability, there are at least three potentially impactful aspects of the laboratory experiments that the numerical model does not consider. First, the simulator does not include the effect of perforation friction and pressure losses along the injection line. Instead, it imposes that the pressure at the wellbore is the same for all fractures and there is no pressure loss between the wellbore and the first element inside each fracture.

Second, as can be seen on the images of experiments, one-dimensional rope-like flow channels appear along the intersection of planes of weakness, that is, intersection of the top and bottom of the fractures with the overlying and base plates of PMMA. This flow effectively comprises a loss of fluid volume from the fractures that is not accounted for in the model.

Third, the storage of fluid in the injection system prior to the start of fracture growth leads to an injection rate that is not constant (as in e.g., Jeffrey & Bungler, 2009). As a result of this and the aforementioned loss of fluid to the flow along the intersections with the horizontal surfaces at the top and bottom of the reservoir, detailed comparison of growth rates is not possible without accounting for non-constant injection. However, the simulations are run with a constant injection rate of 2 ml/min. Consequently, in comparing the experiments to numerical models, we have taken the approach of using the total fracture volume for all five fractures as the independent variable and then selecting it to change in time in such a way that the dominant fracture(s) growth rate of the experiments and the simulations match. The result is a comparison where the agreement between simulation and experiment for the longest fracture is generated by the fitting and is therefore not an independent validation of the simulation results. However, the comparison between data and simulation for the relative growth among the fractures can be evaluated in this way, and, from a practical perspective, simulating the eventual relative size of the fractures is the arguably of greatest importance.

With the model set up and these caveats understood, we next compare the results of the five uniformly narrowly spaced fracture experiment to the numerical predictions. Figure 12a shows the time evolution of average lengths. Comparison shows the localization of growth to the outer fractures is the predominant behavior. The experiment and model are therefore very similar qualitatively, but with the simulation results showing slightly longer fractures than the experiment, which is probably attributable to uncertainty in the actual volume injected in the experiments and fluid loss to the rope-like channels. Furthermore, in both experiment and model a modest favoring of the central fracture, Frac-3, relative to its neighboring fractures, Frac-2 and Frac-4 is visible; however, this favoring is slightly less pronounced in the model than in the experiments.

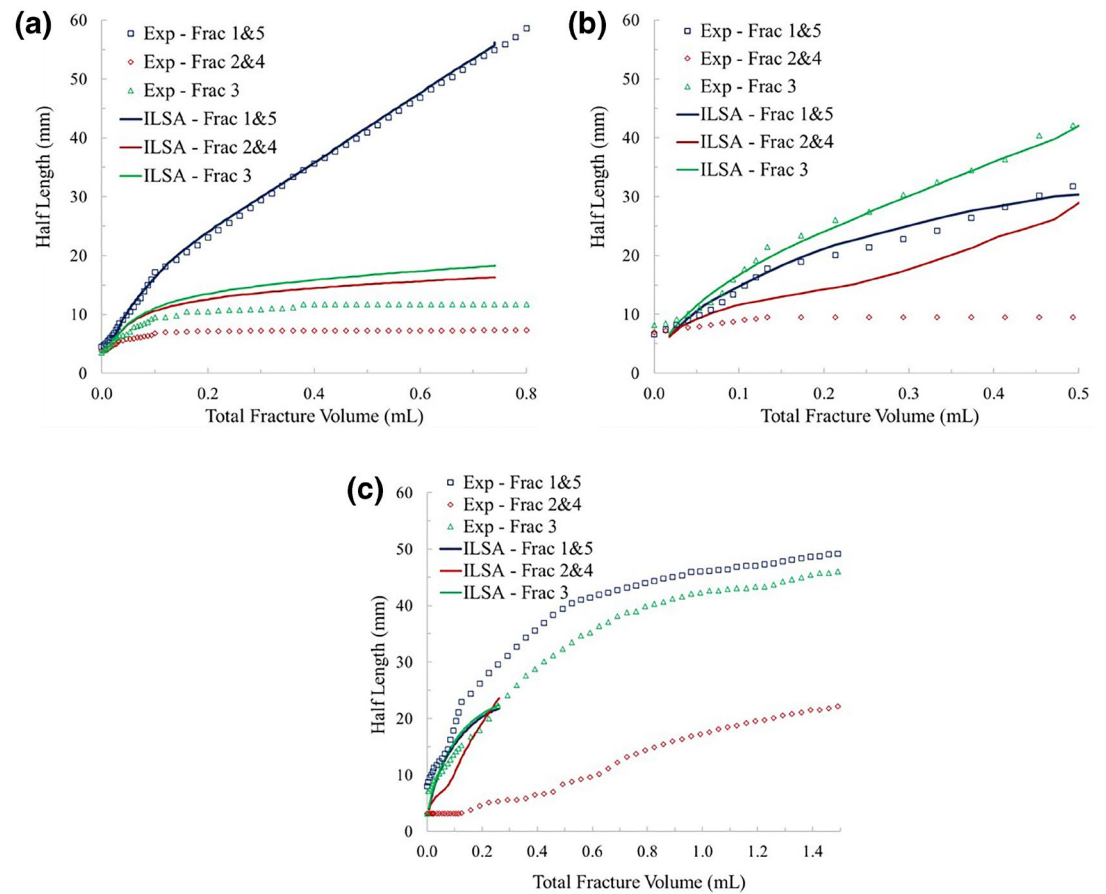


Figure 12. Comparison between experiments and simulation results in terms of fracture half-length versus total injected volume are given in (a) for five uniformly narrowly spaced fractures and (b) for five nonuniformly spaced fractures. (c) For five nonuniformly narrowly spaced fractures.

Next, we consider the five nonuniformly spaced fracture experiment in comparison to the numerical simulation. The comparison in Figure 12b indicates dominance of Frac-3 in both experiment and model. Moreover, the simulation predicts that after a time period where outer fractures and central fracture dominate growth, Frac-2 and Frac-4 catches up to the outer fractures. In the experiments, however, these fractures remain small. As discussed later, it is possible that this is an issue of timing whereby the growth of Frac-2 and Frac-4 in the experiments could have been missed if, for example, details of the non-constant injection rate would lead it to occur later than predicted by the model. If this was the case, then the growth of these fractures would not be observed because the experiment was already stopped because the longer fractures had already reached the specimen boundary.

The hypothesis, then, behind the five nonuniformly narrowly spaced fracture case is that by moving the fractures closer together, the growth of Frac-2 and Frac-4 would occur earlier relative to the arrival of the longer fractures at the edge of the specimen. Indeed, the simulations (Figure 12c) support this hypothesis, with Frac-2 and Frac-4 on track to catch Frac-1 and Frac-5 at an injected volume that is around one fifth of the volume required for the case with wider non-uniform spacing (Figure 12b). Note that the simulation is presented only for rather early time because the narrow spacing necessitates a very fine mesh and hence the computation times become impractical (order of months to years) in order to reach full experimental fracture geometry.

The comparison between the experiments and simulations for the case of five non-uniform narrowly spaced fractures bears some important similarities. First, in both cases, fractures 1, 3, and 5 are similar in length. In the simulation Frac-3 is slightly longer than Frac-1 and Frac-5, while in the experiment Frac-3 is intermediate between the other two (Figure 11) with the average of Frac-1 and Frac-5 tracking slightly above Frac-3.

However, more importantly, the simulations and experiments both show Frac-2 and Frac-4 growing later in the injection time. In the simulations, these two fractures grow together in perfect symmetry. In the experiments (Figure 11), Frac-4 commences growth before Frac-2. It is interesting, though, that Frac-2/4 in the simulations attains a velocity that is greater than the other three fractures. A similar behavior is observed in the experiments, whether viewing Frac-2 and Frac-4 individually (Figure 11) or their average (Figure 12c). The main difference, then, between the experiments and the simulations is the time at which Frac-2 and Frac-4 commence growth. In the experiments there is an additional delay. This observation suggests that experimental imperfections, including non-constant injection rate, probably has the most notable impact on timing of the growth of Frac-2 and Frac-4 relative to simulations where there are no non-symmetries or imperfections to perturb the system. Hence, it points to a useful direction of *in silico* experimentation to investigate sensitivity of simulations to perturbations in symmetry, uniformity of material properties and stresses, and non-constant injection rate.

5. Discussion

This study first shows that when three hydraulic fractures grow with a spacing to height ratio of 0.76 (36.5 mm spacing between each fracture), there is no clear suppression of the middle fracture. The dominance of Frac-1, nearest to the injection point, may be indicating that pressure loss in the injection hole from one inlet to another is the main determinant of which fracture grows the most rapidly. On the other hand, for an array of three uniformly spaced hydraulic fractures with closer spacing (12 mm spacing between each fracture so that the spacing to height ratio is reduced to 0.25), the middle fracture is suppressed. This suppression is presumably evidence of stress shadowing by the outer fractures and leads to the central fracture having a final half-length that is approximately one seventh that of the outer fractures.

The experiments additionally show suppression of the middle three fractures in cases of five uniformly spaced fractures with spacing to height ratio at 0.25 (12–12–12–12 mm for the four spaces separating the five fractures). Accordingly, fracture growth is localized in the outer fractures. Interestingly, the suppression of the central fracture, Frac-3, is slightly less than its neighboring inner fractures, Frac-2 and Frac-4, presumably because Frac-3 is farther from the largest fractures, Frac-1 and Frac-5.

Having observed the often-predicted stress shadow suppression of the central fractures in uniformly and narrowly spaced arrays of hydraulic fractures, the experiments then explore the impact of nonuniform spacing and varying viscosity on central fracture suppression. The first observations come from experiments in which the spacing between five fractures are changed such that Frac-2 and Frac-4 are closer to the outer fractures with a spacing to height ratio of 0.175 (8.4–16–16–8.4 mm spacings). In this case, the middle fracture, Frac-3, grows to be the largest fracture in the array, with Frac-1 and Frac-5 slightly shorter than Frac-3. Growth of Frac-2 and Frac-4 is slightly larger than they were in the uniformly spaced case, but are still substantially suppressed compared to the other three fractures.

In the same geometry, injecting lower viscosity fluid reduces the effect of stress shadowing on inner fractures; however it also causes less geometric stability in their growth, suggesting increasing sensitivity to small variations in notch and block surface topology as well as slight nonuniformity of stress application that is inevitable in laboratory experiments.

Finally, and perhaps most interestingly, all fractures are observed to grow, even at very close spacing, when the spacing between the Frac-2, Frac-3 and Frac-4 are kept nonuniform in similar ratios, but reduced approximately by half such that the spacing to height ratios are 0.09 between Frac-2 and Frac-1 (i.e., 4.2–8.1–8.1–4.2 mm spaces). This is striking because it shows the ability to reduce the suppression of inner fractures due to stress shadowing by moving fractures closer together. This phenomenon requires a suitable nonuniform spacing, chosen so as to uniformly distribute the impacts of stress shadowing to all fractures (after Peirce and Bunger, 2015).

Considering potential practical implications, the final total of the fracture half lengths is increased in the 4.2–8.1–8.1–4.2 mm cases by 60% compared to the total half lengths in the 12–12–12–12 mm cases. This implies the potential to generate considerably more fracture surface area, and hence production, in a smaller section of well.

As mentioned before, each case presented in this paper was performed 3–5 times to ensure that we get consistent results. All the repeated experiments except the five nonuniformly spaced fractures experiments with glycerin as fracturing fluid showed almost identical results. The repeated experiments of three uniformly widely spaced fractures showed no clear suppression of middle fracture. Three uniformly narrowly spaced fractures and five uniformly narrowly spaced fractures always resulted in the dominant growth of outer fractures and suppression of inner fractures. Three out of five repeated experiments of five nonuniformly spaced fractures case indicated similar results to the ones presented in this paper with outer fractures and middle fracture's growth suppressing the growth of Frac-2 and Frac-4. Injecting glycerin into the same geometry caused instability among the fractures. Only one out of five repeated experiments showed very similar results to the results presented in this paper. It is also important to note that all repeated experiments with glycerin as fracturing fluid showed instable geometry in fracture's growths. Finally, last case presented in this paper were repeated three times. All of them showed similar results with more growth among all five fractures with Frac-2 being the smallest in the array.

6. Conclusions

This paper presents results from a series of experiments analyzing the simultaneous development of hydraulic fractures analogous to the growth of hydraulic fractures from multiple perforations in a single stage. These experiments confirm and provide new opportunities to observe and measure details of hydraulic fracture growth impacted by the phenomenon of stress shadowing. Recall that stress shadowing refers to suppression of fractures in regions that are subjected to increasing compressive stresses caused by the growth of other hydraulic fractures. Accordingly, five different cases have been studied with spacing (between the fractures) to height (of central layer) ratio varying from 0.09 to 0.76. Furthermore, the effect of viscosity on reducing the stress interaction between fractures is examined in one of the cases. Experiments with lower viscosity injection fluid indicate that while lowering the viscosity can reduce the effect of stress shadowing on inner fractures; it can also cause less geometric stability in their growth, suggesting increasing sensitivity to small variations in specimen conditions that is inevitable in laboratory experiments.

In addition to the experiments, a fully coupled, parallel-planar simulator, ILSA, is used to compare the experiment results to numerical model predictions. The focus of this comparison is specifically on two contrasting experiments: (1) five uniformly spaced fractures experiment where inner fractures are suppressed due to stress shadowing. (2) Five fractures in a nonuniform array experiment where all fractures show robust growth.

Consistent with the numerical model's predictions, these experiments show that when the fractures are uniformly distributed in an array, substantial growth of outer fracture's induce additional compressive stresses on inner fractures and consequently stunt their growth. The experiments and model agree all the way to the detail of the slight favoring of the central fracture, Frac-3, over its neighbors, Frac-2 and Frac-4.

Moreover, the results show that the stress shadowing effect that is pronounced in the uniformly spaced array can be reduced by optimized nonuniform fracture spacing. The simulations and experiments both show robust growth of not only Frac-1 and Frac-5 (as in the uniformly spaced case), but also of Frac-3, with Frac-3 sometimes even exceeding the length of Frac-1 and Frac-5 for certain non-uniform spacing configurations. Furthermore, both experiments and simulations show that Frac-2 and Frac-4 accelerate growth as the injection continues and eventually achieve a velocity that exceeds the other three fractures. While the timing of this acceleration of Frac-2 and Frac-4 appears to be sensitive to experimental perturbations, the qualitative similarities remain and provide the first experimental evidence that such delayed growth of Frac-2 and Frac-4 is possible and not just an artifact observed in fully coupled hydraulic fracture simulations.

Taken together, the experiments most notably provide laboratory-scale demonstration of what is possible. Specifically, these demonstrate potential to substantially impact growth behavior of hydraulic fractures by placing them in nonuniform spacing configurations, in a manner which is guided by mechanical models. When chosen in such a way, non-uniform spacing of hydraulic fractures has the ability to promote substantially more uniform growth among the array of fractures and considerably larger total generated fracture surface area.

Data Availability Statement

Data used to generate the figures in this paper can be downloaded from <http://d-scholarship.pitt.edu/id/eprint/38828>.

Appendix A: Specimen Preparation

PMMA blocks are cut and machined to appropriate sizes. To achieve the final tolerances, a surface grinder with a 254 mm diameter diamond wheel is used to provide smooth and precision ground surfaces. Fractures are initiated from a manufactured notch at the base of the flat-bottomed injection holes. For all PMMA blocks, the notches are created with a 3° taper end mill with a 6.35 mm diameter. Depths of the notches created for five nonuniformly narrowly spaced fractures experiment is smaller to accommodate the thinner layers. Schematics of these manufactured notches at the base of the injection holes are given in Figure A1.

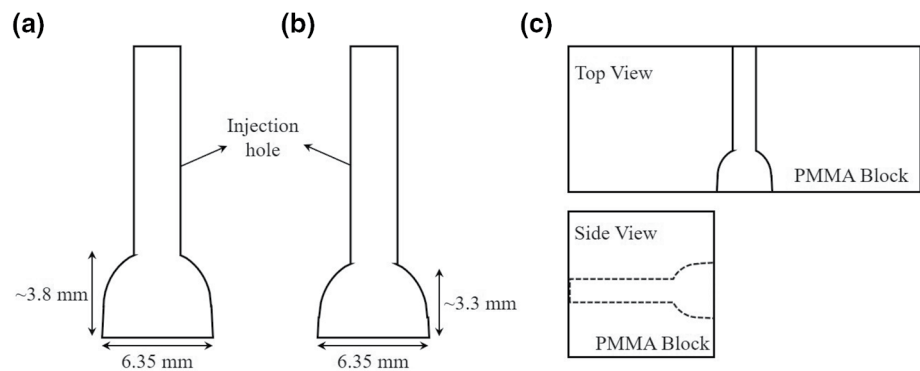


Figure A1. Schematic of the injection hole with manufactured flaw: for the first four cases (a), for the last case (b), and injection hole with manufacture flaw in a PMMA block – top view and side view (c).

Appendix B: Pressure Loss Calculations

Darcy-Weisbach equation for laminar flow in a cylindrical pipe of uniform diameter is used to estimate the pressure drop across the wellbore as the fluid reaches to the last fracture in the array from the first fracture, Frac-1.

$$\frac{\Delta P}{L} = \frac{128}{\pi} \frac{\mu Q}{D^4} \quad (\text{B1})$$

where the pressure loss per unit length $\Delta P / L$ (Pa/m) is a function of: μ , the dynamic viscosity of the fluid (Pa-s); D , the internal diameter of the pipe (m) and Q , the volumetric flow rate (m^3/s).

Acknowledgments

This project is funded by the National Science Foundation under Grant no. 1645246. This support is gratefully acknowledged. The outstanding technical contributions of Charles Hager (University of Pittsburgh) are also recognized.

References

- AlTammar, M. J., Sharma, M. M., & Manchanda, R. (2018). The effect of pore pressure on hydraulic fracture growth: An experimental study. *Rock Mechanics and Rock Engineering*, 51(9), 2709–2732. <https://doi.org/10.1007/s00603-018-1500-7>
- Bunger, A. P. (2005). *Near-surface hydraulic fracture*, (Doctoral dissertation). University of Minnesota, ProQuest Dissertations Publishing.
- Bunger, A. P. (2006). A photometry method for measuring the opening of fluid-filled fractures. *Measurement Science and Technology*, 17(12), 3237–3244. <https://doi.org/10.1088/0957-0233/17/12/006>
- Bunger, A. P., & Cardella, D. J. (2015). Spatial distribution of production in a Marcellus Shale well: Evidence for hydraulic fracture stress interaction. *Journal of Petroleum Science and Engineering*, 133, 162–166. <https://doi.org/10.1016/j.petrol.2015.05.021>
- Bunger, A. P., & Detournay, E. (2008). Experimental validation of the tip asymptotic for a fluid-driven crack. *Journal of the Mechanics and Physics of Solids*, 56(11), 3101–3115. <https://doi.org/10.1016/j.jmps.2008.08.006>

- Bunger, A. P., Menand, T., Cruden, A., Zhang, X., & Halls, H. (2013). Analytical predictions for a natural spacing within dyke swarms. *Earth and Planetary Science Letters*, 375, 270–279. <https://doi.org/10.1016/j.epsl.2013.05.044>
- Bunger, A. P., Zhang, X., & R. G. Jeffrey (2012). Parameters affecting the interaction among closely spaced hydraulic fractures. *SPE Journal* 17(01), 292–306. <https://doi.org/10.2118/140426-PA>
- Castonguay, S. T., Mear, M. E., Dean, R. H., & Schmidt, J. H. (2013). Predictions of the growth of multiple interacting hydraulic fractures in three dimensions. Paper presented at *SPE Annual Technical Conference and Exhibition*. New Orleans, LA: Society of Petroleum Engineers.
- Cheng, C., & Bunger, A. P. (2019). Optimizing fluid viscosity for systems of multiple hydraulic fractures. *AIChE Journal*, 65(5), e16564. <https://doi.org/10.1002/aic.16564>
- Cipolla, C. L., Lewis, R. E., Maxwell, S. C., & Mack, M. G. (2011). Appraising unconventional resource plays: Separating reservoir quality from completion effectiveness. Paper presented at *International Petroleum Technology Conference*. Bangkok: International Petroleum Technology Conference, IPTC-14677-MS.
- Damjanac, B., Maxwell, S., Pirayehgar, A., & Torres, M. (2018). Numerical study of stress shadowing effect on fracture initiation and interaction between perforation clusters. Paper presented at *Unconventional Resources Technology Conference, Houston, Texas, 23-25 July 2018*. Houston, TX: Society of Exploration Geophysicists, American Association of Petroleum.
- Detournay, E. (2016). Mechanics of hydraulic fractures. *Annual Review of Fluid Mechanics*, 48(1), 311–339. <https://doi.org/10.1146/annurev-fluid-010814-014736>
- Detournay, E., & Peirce, A. (2014). On the moving boundary conditions for a hydraulic fracture. *International Journal of Engineering Science*, 84, 147–155. <https://doi.org/10.1016/j.ijengsci.2014.06.010>
- El Rabaa, W. (1989). Experimental study of hydraulic fracture geometry initiated from horizontal wells. Paper presented at *SPE Annual Technical Conference and Exhibition*. San Antonio, TX: Society of Petroleum Engineers.
- Fisher, M., Heinze, J., Harris, C., Davidson, B., Wright, C., & Dunn, K. (2004). Optimizing horizontal completion techniques in the Barnett shale using microseismic fracture mapping. Paper presented at *SPE Annual Technical Conference and Exhibition*. Houston, TX: Society of Petroleum Engineers.
- Gao, H., & Rice, J. R. (1987). Somewhat circular tensile cracks. *International Journal of Fracture*, 33(3), 155–174. <https://doi.org/10.1007/BF00013168>
- Garagash, D., & Detournay, E. (2000). The tip region of a fluid-driven fracture in an elastic medium. *Journal of Applied Mechanics*, 67(1), 183–192.
- Jeffrey, R. G., & Bunger, A. (2009). A detailed comparison of experimental and numerical data on hydraulic fracture height growth through stress contrasts. *SPE Journal*, 14(3), 413–422. <https://doi.org/10.2118/106030-PA>
- Kresse, O., Weng, X., Gu, H., & Wu, R. (2013). Numerical modeling of hydraulic fractures interaction in complex naturally fractured formations. *Rock Mechanics and Rock Engineering*, 46(3), 555–568.
- Lagrone, K. W., & Rasmussen, J. W. (1963). A new development in completion methods—the limited entry technique. *Journal of Petroleum Technology*, 15(7), 695–702. <https://doi.org/10.2118/530-PA>
- Lakirouhani, A., Detournay, E., & Bunger, A. P. (2016). A reassessment of in situ stress determination by hydraulic fracturing. *Geophysical Journal International*, 205(3), 1859–1873. <https://doi.org/10.1093/gji/ggw132>
- Lecampion, B., & Desroches, J. (2015). Robustness to formation geological heterogeneities of the limited entry technique for multi-stage fracturing of horizontal wells. *Rock Mechanics and Rock Engineering*, 48(6), 2637–2644. <https://doi.org/10.1007/s00603-015-0836-5>
- Lhomme, T., Detournay, E., & Jeffrey, R. G. (2005). Effect of fluid compressibility and borehole on the initiation and propagation of a transverse hydraulic fracture. *Strength, Fracture and Complexity*, 3(2–4), 149–162.
- Meyer, B. R., & Bazan, L. W. (2011). A discrete fracture network model for hydraulically induced fractures—theory, parametric and case studies. Paper presented at *SPE Hydraulic Fracturing Technology Conference*. The Woodlands, TX: Society of Petroleum Engineers.
- Miller, C. K., Waters, G. A., & Rylander, E. I. (2011). Evaluation of production log data from horizontal wells drilled in organic shales. Paper presented at *North American Unconventional Gas Conference and Exhibition*. The Woodlands, TX: Society of Petroleum Engineers.
- Miskimins, J., Barree, R., Wheaton*, B., Wood, D., & Lowe, T. (2014). Integration of distributed temperature and distributed acoustic survey results with hydraulic fracture modeling: A case study in the Woodford shale. Paper presented at *Unconventional Resources Technology Conference, Denver, Colorado, 25-27 August 2014*. Society of Exploration Geophysicists, American Association of Petroleum.
- Molenaar, M. M., Hill, D., Webster, P., Fidan, E., & Birch, B. (2012). First downhole application of distributed acoustic sensing for hydraulic-fracturing monitoring and diagnostics. *SPE Drilling and Completion*, 27(01), 32–38. <https://doi.org/10.2118/140561-PA>
- Nordgren, R. (1972). Propagation of a vertical hydraulic fracture. *Society of Petroleum Engineers Journal*, 12(04), 306–314. <https://doi.org/10.2118/3009-PA>
- Olson, J. (2008). Multi-fracture propagation modeling: Applications to hydraulic fracturing in shales and tight gas sands. Paper presented at *The 42nd US Rock Mechanics Symposium (USRMS)*. San Francisco, CA: American Rock Mechanics Association.
- Peirce, A., & Bunger, A. (2015). Interference fracturing: Nonuniform distributions of perforation clusters that promote simultaneous growth of multiple hydraulic fractures. *SPE Journal*, 20(02), 384–395. <https://doi.org/10.2118/172500-PA>
- Peirce, A., & Detournay, E. (2008). An implicit level set method for modeling hydraulically driven fractures. *Computer Methods in Applied Mechanics and Engineering*, 197(33), 2858–2885. <https://doi.org/10.1016/j.cma.2008.01.013>
- Peirce, A. P., & Dontsov, E. V. (2017). Modeling the effect of turbulence on the simultaneous propagation of multiple parallel hydraulic fractures. Paper presented at *51st U.S. Rock Mechanics/Geomechanics Symposium*. San Francisco, CA: American Rock Mechanics Association.
- Perkins, T., & Kern, L. (1961). Widths of hydraulic fractures. *Journal of Petroleum Technology*, 13(09), 937–949. <https://doi.org/10.2118/89-PA>
- Roussel, N. P., & Sharma, M. M. (2011). Optimizing fracture spacing and sequencing in horizontal-well fracturing. *SPE Production & Operations*, 26(2), 173–184. <https://doi.org/10.2118/127986-PA>
- Salah, M., & Ibrahim, M. (2018). Engineered fracture spacing staging and perforation cluster spacing optimization for multistage fracturing horizontal wells. Paper presented at *SPE Annual Technical Conference and Exhibition*. Dallas, TX: Society of Petroleum Engineers.
- Savitski, A. A., & Detournay, E. (2002). Propagation of a penny-shaped fluid-driven fracture in an impermeable rock: Asymptotic solutions. *International Journal of Solids and Structures*, 39(26), 6311–6337. [https://doi.org/10.1016/S0020-7683\(02\)00492-4](https://doi.org/10.1016/S0020-7683(02)00492-4)
- Simonson, E. R., Abou-Sayed, A. S., & Clifton, R. J. (1978). Containment of massive hydraulic fractures. *Society of Petroleum Engineers Journal*, 18(1), 27–32. <https://doi.org/10.2118/6089-PA>
- Slocombe, R., Acock, A., Chadwick, C., Wigger, E., Viswanathan, A., Fisher, K., & (2013). Eagle Ford completion optimization strategies using horizontal logging data. Paper presented at *Unconventional Resources Technology Conference*. Denver, CO: Society of Exploration Geophysicists.

- Ugueto, C., Gustavo, A., Huckabee, P. T., Molenaar, M. M., Wyker, B., & Somanchi, K. (2016). Perforation cluster efficiency of cemented plug and perf limited entry completions; Insights from fiber optics diagnostics. *Paper presented at SPE Hydraulic Fracturing Technology Conference*. The Woodlands, TX: Society of Petroleum Engineers.
- Wheaton, B., Haustveit, K., Deeg, W., Miskimins, J., & Barree, R. (2016). A case study of completion effectiveness in the eagle ford shale using DAS/DTS observations and hydraulic fracture modeling. *Paper presented at SPE Hydraulic Fracturing Technology Conference*. The Woodlands, TX: Society of Petroleum Engineers.
- Xing, P., Yoshioka, K., Adachi, J., El-Fayoumi, A., & Bunger, A. P. (2017). Laboratory measurement of tip and global behavior for zero-toughness hydraulic fractures with circular and blade-shaped (PKN) geometry. *Journal of the Mechanics and Physics of Solids*, *104*, 172–186. <https://doi.org/10.1016/j.jmps.2017.04.013>
- Xing, P., Yoshioka, K., Adachi, J., El-Fayoumi, A., & Bunger, A. P. (2018). Laboratory demonstration of hydraulic fracture height growth across weak discontinuities. *Geophysics*, *83*(2), MR93–MR105. <https://doi.org/10.1190/geo2016-0713.1>
- Zia, H., & Lecampion, B. (2017). Propagation of a height contained hydraulic fracture in turbulent flow regimes. *International Journal of Solids and Structures*, *110–111*, 265–278. <https://doi.org/10.1016/j.ijsolstr.2016.12.029>
- Zolfaghari, N., & Bunger, A. P. (2019). Numerical model for a penny-shaped hydraulic fracture driven by laminar/turbulent fluid in an impermeable rock. *International Journal of Solids and Structures*, *158*, 128–140. <https://doi.org/10.1016/j.ijsolstr.2018.09.003>